BULLETIN OF THE POLISH ACADEMY OF SCIENCES
TECHNICAL SCIENCES, Vol. 67, No. 2, 2019
DOI: 10.24425/bpas.2019.128115

Aggregate segmentation of asphaltic mixes using digital image processing

O.J. REYES-ORTIZ*, M. MEJÍA, and J.S. USECHE-CASTELBLANCO

Nueva Granada Military University, Faculty of Engineering, Bogotá D.C., Colombia

Abstract. The study of the different engineering materials according to their mechanical and dynamic characteristics has become an area of research interest in recent years. Several studies have verified that the mechanical properties of the material are directly affected by the distribution and size of the particles that compose it. Such is the case of asphalt mixtures. For this reason, different digital tools have been developed in order to be able to detect the structural components of the elements in a precise, clear and efficient manner. In this work, a segmentation model is developed for different types of dense-graded asphalt mixtures with grain sizes from 9.5 mm to 0.0075 mm, using sieve size reconstruction of the laboratory production curve. The laboratory curve is used to validate the particles detection model that uses morphological operations for elements separation. All this with the objective of developing a versatile tool for the analysis and study of pavement structures in a non-destructive test. The results show that the model presented in this work is able to segment elements with an area greater than 0.0324 mm^2 and reproduce the sieve size curves of the mixtures with a high percentage of precision.

Key words: digital image processing, asphalt mixtures, morphological operations, particle segmentation.

1. Introduction

Research on structural components and particulates of elements is becoming a field of high importance in engineering [1]. The distribution of particles in the different materials has a direct impact on their mechanical and dynamic behavior, according to Di Maria, Bianconi et al. in [2]. For example, in asphalt mixtures, the homogeneous or random orientation of the aggregate is related to maximum stresses, durability, stability and self-consolidation, among other variables [3].

In order to improve this type of studies, digital tools, using images, have been developed. The photos allow for inspection and obtaining information on samples in a more precise and systematic manner for processes that were previously manual or visual [4, 5]. There are two types of methods for the analysis of images with particles: the direct method, which segments element by element, looking to determine individual shapes or areas, and the indirect one, which analyzes the complete set [6].

According to S. Yin, Y. Qian and M. Gong in [7], direct digital image processing focuses on extracting and understanding from an image as many features as possible of its contents. The process is based on dividing the image into different partitions that represent the studied objects. With the elements segmented using different computational algorithms, those objects are recognized. This way, the main objective is to change the representation of the image through a process that helps make it more understandable and easier to analyze [8, 9].

According to the author of [10], the general steps for digital image processing are thresholding, filtering, segmentation and extraction. Each one of them develops a series of specific operations that allow to obtain the required information from an image. Thresholding allows to create a binary or grayscale image, manipulating the values of the histogram of each color layer defining an intensity range to modify its colors. Filtering uses different mathematical functions to eliminate noise and unnecessary elements. Segmentation is performed through morphological operations that use spatial distribution of the image to separate and define geometries. Finally, extraction implements computational algorithms to classify or interpret the information on image elements [11–13].

Some recent works that have used digital image processing for the segmentation of particles and objects are presented below. In the field of medicine, M. Mejia and M. Alzate [14] developed a tool to aid the diagnosis and examination of peripheral blood smears, segmenting seven different erythrocyte abnormalities using a neural network. The results show a success rate in the classification of 97%, as compared to the manual classification performed by an expert. A work in the field of agriculture presented by Espinoza, Valera et al. [15] presents the segmentation of two pest types that affect the tomato in Spain used a detection support tool. It begins with an adjustment of the histogram of the images and with implementation of digital filters and notes an average identification error of 6%. Two papers have also been presented on the subject of pavements. The first one was developed by Tedeschi and Benedetto [16] and the second by Hyun-Seok and Young-Suk [17]. Both works show the segmentation of different types of cracks using traditional segmentation techniques. As a result, the first system has 93% of accuracy in the recognition of failures. This figure stands at 97.4% for the second paper, which additionally uses artificial intelligence for the classification and extraction of elements.

*e-mail: oscar.reyes@unimilitar.edu.co

Manuscript submitted 2017-12-22, revised 2018-05-03, initially accepted for publication 2018-07-18, published in April 2019.

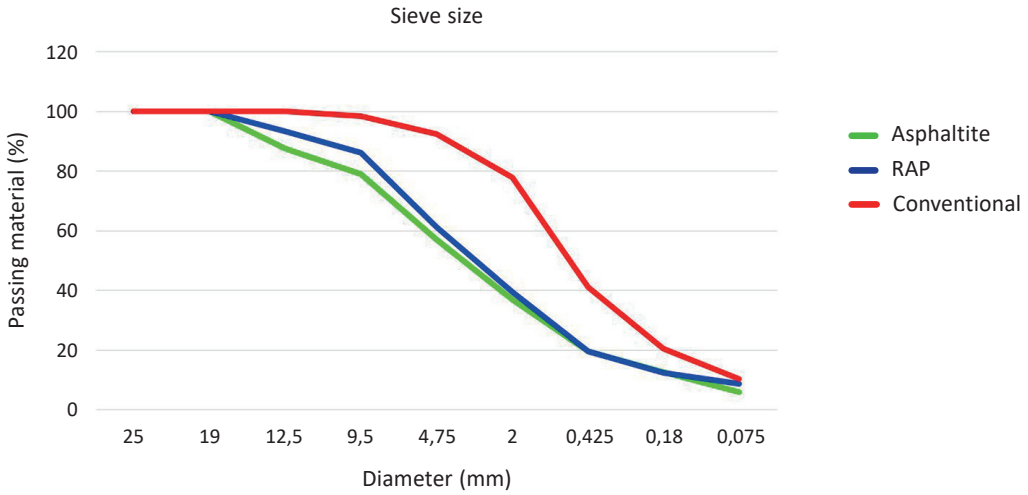

Fig. 1. Sieve size curves

This work presents an implementation of digital image processing for the classification of particles in different types of dense-graded asphalt mixtures. Segmentation separates the elements within a range of 25 to 0.075 mm in size, and results are compared with the laboratory sieve size curves of the samples. The comparison is made to verify the quantity of material that can be recognized and to generate a digital tool for the reconstruction of material percentages. The paper is divided first into a section on methods, where the entire process is shown from image acquisition until aggregate separation. Then in the results section the different error tables are presented for the proposed method to make the relevant conclusions and proposals for future work.

2. Methods and materials

For the development of the work samples of different types of hot mix asphalt are required. A mixture of asphaltite, a conventional MDC-19 and a recycled pavement (RAP) is used under the regulations of the National Roads Institute of Colombia (INVIAS). A gyratory compactor and the sieve size curves presented in Fig. 1 are employed in the manufacturing.

The complete working model used in this work is observed in Fig. 2, where the stages of acquisition, conditioning, presieving, separation and sieving are clearly defined. Matlab®, as a platform of development and programming, is used for handling and processing of images.

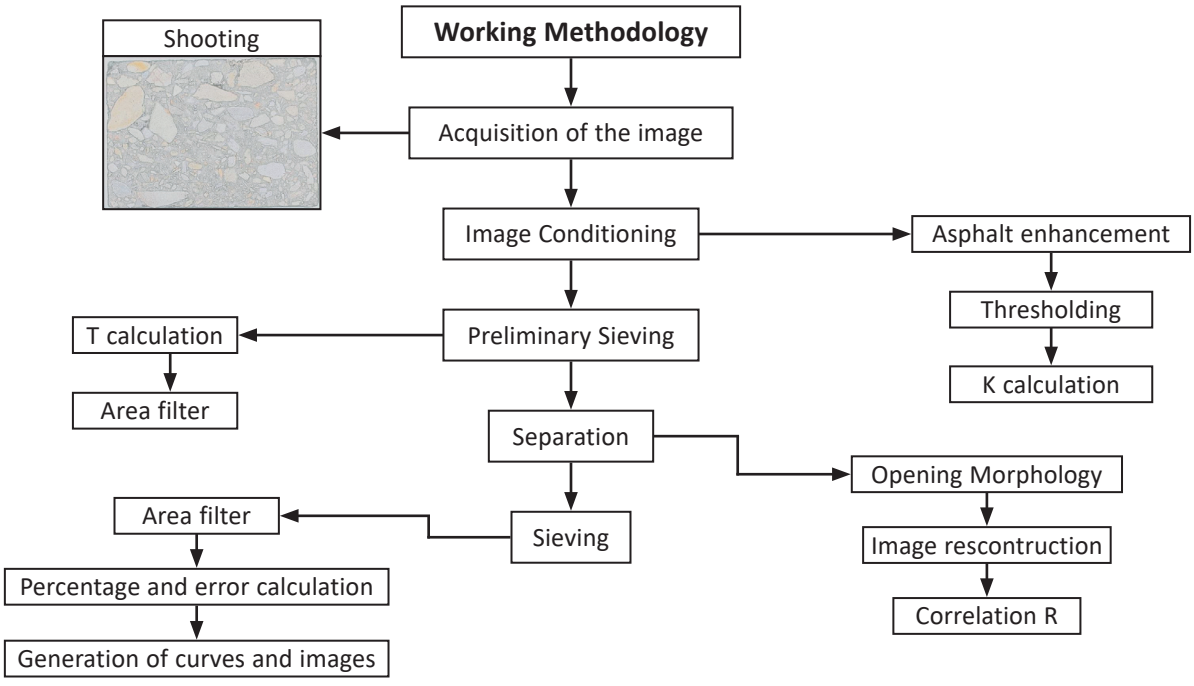

Fig. 2. Working model for aggregate segmentation

Fig. 3. Shooting with a variety of filters: (a) standard, (b) tungsten, (c) oil, (d) watercolor

2.1. Acquisition of image. A conventional 18 Megapixel camera with a precision lens is used to capture the image. The photo is made with different filters, as shown in Fig. 3, to determine the best form of capture. It is necessary to try different filters because asphalt mixtures present some problems such as the confusion of dark stones with the background (paving grade bitumen).

Searching for the filter with which best result is obtained, several critical points are taken into account like the fact that the dark aggregate that can be confused with the asphalt and the contact points that share particles, as shown in Fig. 4. The watercolor filter softens the colors to white and highlights the edges to black. Using this filter, the color difference between the aggregate will not affect the processing and the edge enhancement will help complete preliminary particles separation.

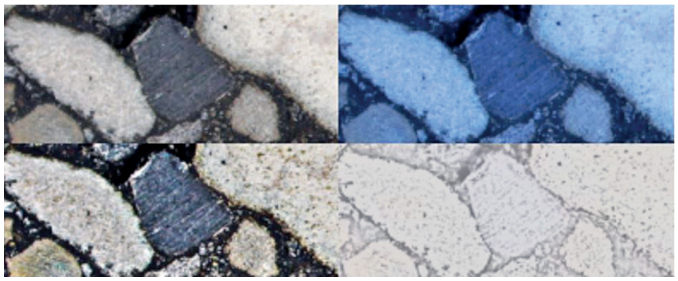

Fig. 4. Critical point of contact and color

The watercolor filter handles a convolution mask which is then scrolled through the image, detecting continuous elements. These are assigned a light color tone while the discontinuities (edges) become darker.

2.2. Image conditioning. Let *Im* be an acquired RGB multilayer image. The values of the layers are modified with a threshold using the part function of (1). The background of the photo is highlighted, sending the dark values to 0 and the aggregate to 1.Thus the new *M* image is created.

$$M(x,y) = \begin{cases} 0 & \textbf{\textit{if}} \quad Im(x,y,1) \ \textbf{\textit{and}} \ Im(x,y,2) \ \textbf{\textit{and}} \ Im \le Vx \\ 1 & \textbf{\textit{if}} \quad \textit{Another case} \end{cases} \tag{1}$$

The threshold value (*Vx*) can change depending on the external disturbances at the moment of taking the photo. In order to maximize inter-class variance, the Otsu method is used, according to [18]. Equation 2 shows the calculation of the variance proposed by the method, in which the maximum value is chosen to obtain the optimum threshold value as observed in (3).

$$\sigma_B^2(t) = \omega_1(t)\left(\mu_1(t) - \mu_T\right)^2 + \omega_2(t)\left(\mu_2(t) - \mu_T\right)^2 \tag{2}$$

$$Vx = Arg \underset{1 \le t \le L}{Max} \left\{\sigma_B^2(t)\right\} \tag{3}$$

Where t are the different color values that pixels can take within the range of the spectrum of the photo and ω_1 and ω_2 are the probability distributions of the image color levels. μ_1 and μ_2 represent the mean for the different classes composed by the color tones and μ_T is the average color intensity of the whole image [19].

For aggregate separation, first the *K* parameter is obtained using (4), which relates the actual size of the sample in millimeters with its representation in pixels. This is calculated by means of measuring the number n of heights in the real element and in the image.

$$K = \frac{\sum_{i=1}^{n} \frac{Photo\ height_i}{Real\ height_i}}{n} = \frac{Pixel}{mm} \tag{4}$$

Then, the total area of the aggregate is calculated using the expression from (5). The function counts white pixels inside the image. This data is necessary to calculate the sieve size percentages later, and to verify the method proposed in the work.

$$Area = \sum_x \sum_y M(x,y) \tag{5}$$

2.3. Preliminary sieving. The separation of the aggregate is done the same way as in the laboratory. The material is passed through a series of sieves, which are elements with a square mesh with a defined pitch length *P*. The sieve retains particles with an area greater than the mesh square. To recreate them digitally, the *K* relation value is used, where a vector *T* is created with the pass areas in pixels using the lengths of the different

sieves presented in millimeters. The calculation of the vector's expression is given in (6).

$$T_i = (PK)^2 \tag{6}$$

Figure 5 shows the distribution the aggregate sizes and the T calculation for nine sieves used in this work. The image is captured of the aggregate passing through the sieves from the largest to the smallest one using a different area filter for each case.

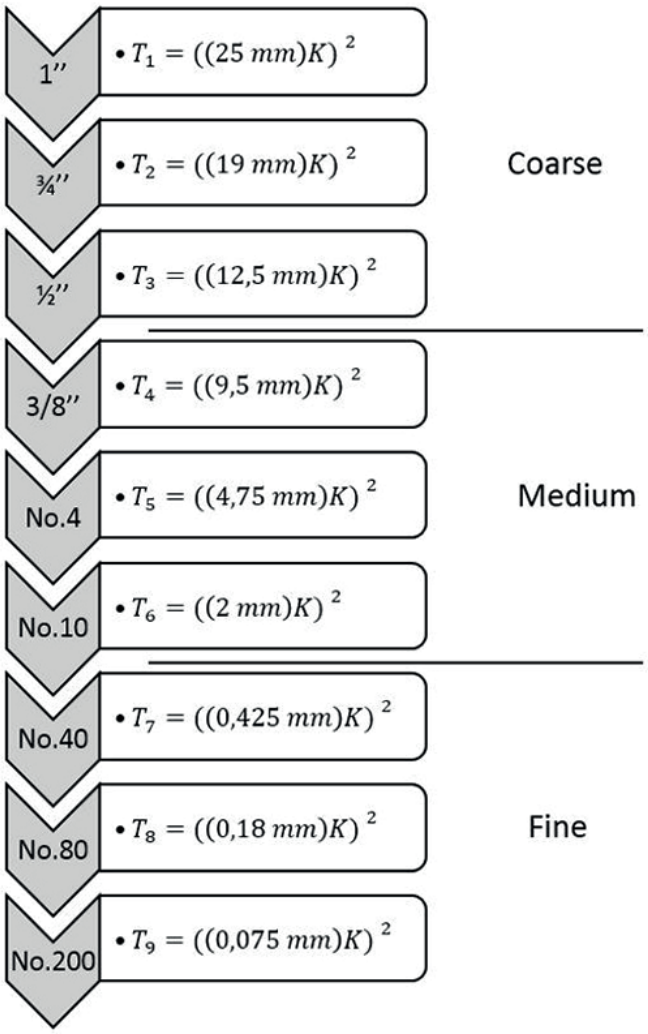

Fig. 5. Calculation of digital sieves

Preliminary sieving uses the values of the vector T to compare them with individual areas of the particles. Each area of the aggregate is calculated using the same function of equation 5, which was also used for the calculation of the total area. All the aggregate goes through the sieves from 1" up to No. 200. A new image is created with the material that didn´t pass through the sieve. These particles are subtracted from the total, to which the following sieve will be applied.

The main goal of this section is to separate the elements into subgroups to apply morphological operations. In order to separate the aggregate of 25 mm in size, it is necessary to have a morphological structural element larger than the one used with the particles of 0.425 mm in size. That is the reason for which the elements are divided into different images before any operation. Figure 6 shows an example of preliminary sieving of 12.5 mm-sized particles, where it is observed how it is necessary to apply morphological operations to separate the particles that remain together.

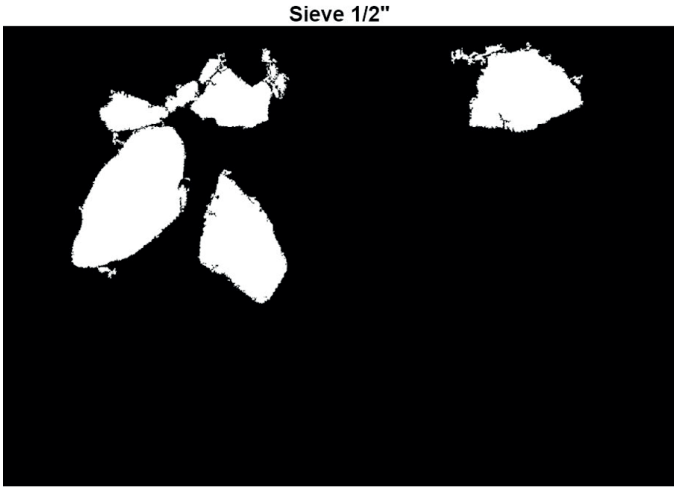

Fig. 6. Preliminary sieving

2.4. Segmentation. For each of the resulting images of pre-sieving, the opening morphological operation is used in order to define, separate, segment or eliminate unnecessary particles [20]. The mathematical model for the morphological operation of opening is seen in (7). This is an operation composed of erosion followed by dilation that helps separate bound elements without affecting their total area [21].

$$\begin{aligned} &\textit{Erosion: } \varepsilon_B(A) = A \ominus B = \{z \,|\, B_z \subseteq A\} \\ &\textit{Dilation: } \delta_B(A) = A \oplus B = \{z \,|\, B_z \cap A \neq \emptyset\} \\ &\textit{Opening: } \gamma_B(A) = A \circ B = \delta_B\big(\varepsilon_B(A)\big) \end{aligned} \tag{7}$$

A is the image, B represent the structuring element, z is a pixel position (x, y) and B_z is the structural element B centered at z.

Erosion is the result of checking whether B_z is completely enclosed in A. If that is not the case, the pixel $A(z)$ is not contained in $\varepsilon_B(A)$. In the dilation, if A and B_z overlap by at least one element, the pixel $A(z)$ is contained in $\delta_B(A)$. It is more intuitive when B is viewed as a convolution mask that slides over image A in all its positions [22, 23].

The sizes of the morphological structural elements increase from the smallest to the largest sieve. It is necessary to watch the size of the structures to avoid the elimination of small particles

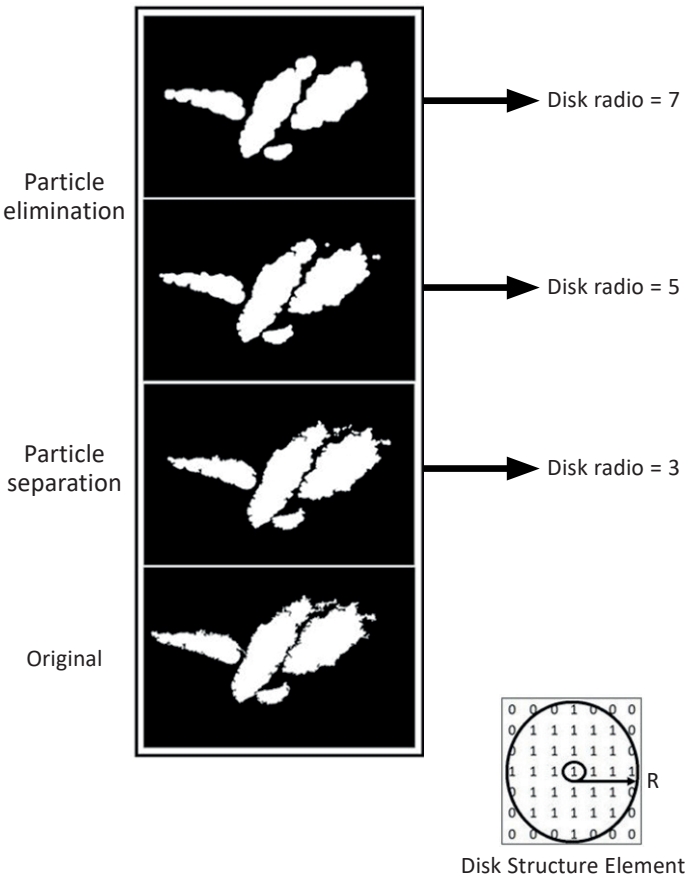

Fig. 7. Opening morphological application

joined with larger aggregates. In Fig. 7, the impact of different size values for the separation of the aggregate is observed.

Once the morphological operations have been applied to all the pre-sieving images, a single image containing all the separated particles of the sample is reconstructed. Using the operations, the elements of the image are modified and some are even eliminated. For this reason, the original and reconstructed image are compared through the correlation function (8) used by Xiangzhi Bai in [24]. When the modification exceeds 5%, the values of morphological structural element sizes must be reduced.

$$r = \frac{\Sigma_x \Sigma_y \left(F_{xy} - \bar{F}\right)\left(Ft_{xy} - \overline{Ft}\right)}{\sqrt{\Sigma_x \Sigma_y \left(F_{xy} - \bar{F}\right)^2 \left(Ft_{xy} - \overline{Ft}\right)^2}} \tag{8}$$

Where F_{xy} and Ft_{xy} are the images to be compared and $\bar{F}$ and $\overline{Ft}$ are the averages of the elements for each image. If the correlation is greater than 95%, the final sieving is performed with filtering the area of each particle A_j of the reconstructed image. The filters use a pass window defined by the relations of the vector T.

2.5. Sieving. A general working scheme of a sieve is presented in Fig. 8, wherein the retained material is subtracted from the

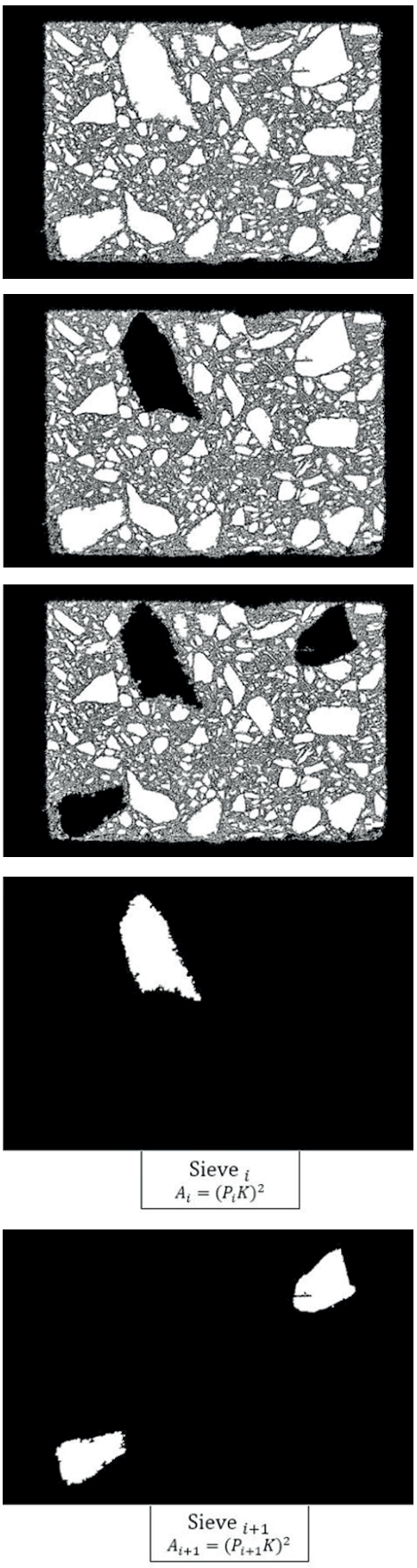

Fig. 8. Digital sieving

total aggregate. Sieving is independent of the shape of the aggregate. The area in pixels that occupies each particle in the photo is always compared with each sieve pass area.

The area of the material retained per sieve is calculated to assign a percentage based on the total area of the aggregate previously calculated. Using formula (9), the percentages are generated taking into account the material that has already been removed from the previous sieves. For the calculation of the error, the real percentages are compared with the calculated values. The normalized error function that is used in this case can be seen in (10).

$$Percentage_1 = 100$$
$$Percentage_1 = Percentage_{i-1} - 100\left(\frac{SieveArea_i}{TotalArea}\right) \quad (9)$$

$$Error_1 = \frac{100\,|RealPercentage_i - Percentage_i|}{RealPercentage_i} \quad (10)$$

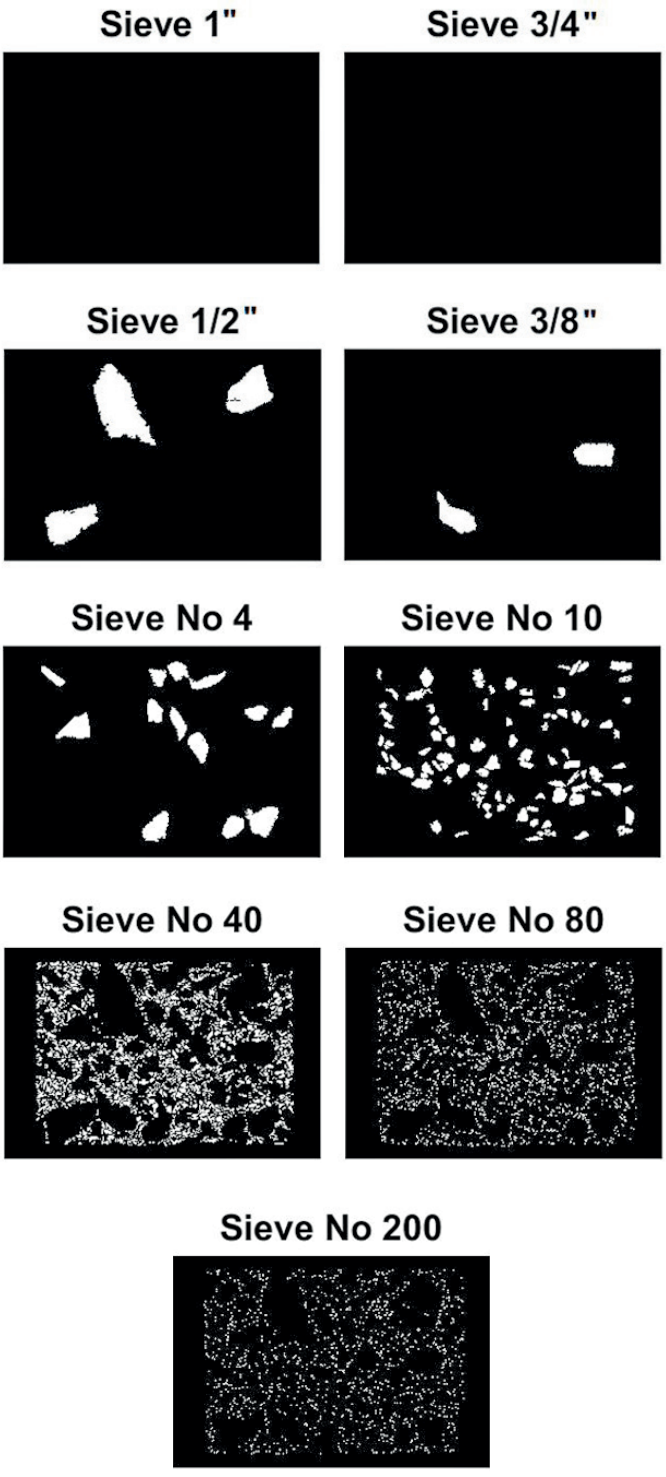

Fig. 9. Segmentation by sieves

3. Results

The segmentation and sieve size reconstruction model is applied for 40 samples of different types, including conventional samples, asphaltite samples characterized by their fine aggregate of 9.5 to 0.075 mm in size and RAP (recycled asphalt pavement). Fig. 9 shows the result of segmentation of a conventional sample and its distribution in the different sieves.

The reconstruction of the sieve size curve for each type of mixture can be seen in Figs 10, 11 and 12. In them, the passing material is the percentage of the aggregate total area that passes to the next, smaller sieve. For this reason, we naturally begin with 100% of the particles. On the other hand, the diameter variable is the pitch length P for each sieve in a logarithmic scale. *Mx*, *RAPx* and *AFx* are the analyzed samples of the different mixtures.

Table 1 shows consolidation of the error for each type of mixture as per different sieve sizes. The reconstruction of the particles made for elements up to the No. 80 sieve have an average error of 2.98% and the error grows up to 7.26% on

Table 1
Consolidated error

Sieve / Samples	Reconstruction error percentage (%)			
	RAP	*Asphaltite*	*Conventional*	*Average*
1”	0.00	0.00	0.00	0.00
3/4”	0.00	0.00	0.00	0.00
1/2”	2.61	0.00	3.43	2.01
3/8”	3.72	1.71	3.72	3.04
No 4	2.81	1.59	3.70	2.69
No 10	7.25	3.79	2.55	4.51
No 40	1.73	2.07	2.98	2.20
No 80	2.84	3.11	1.95	2.62
No 200	9.11	29.50	55.62	31.40
Error up to No. 80	3.46	2.45	3.04	2.98
Error up to No. 200	4.27	6.96	10.55	7.26

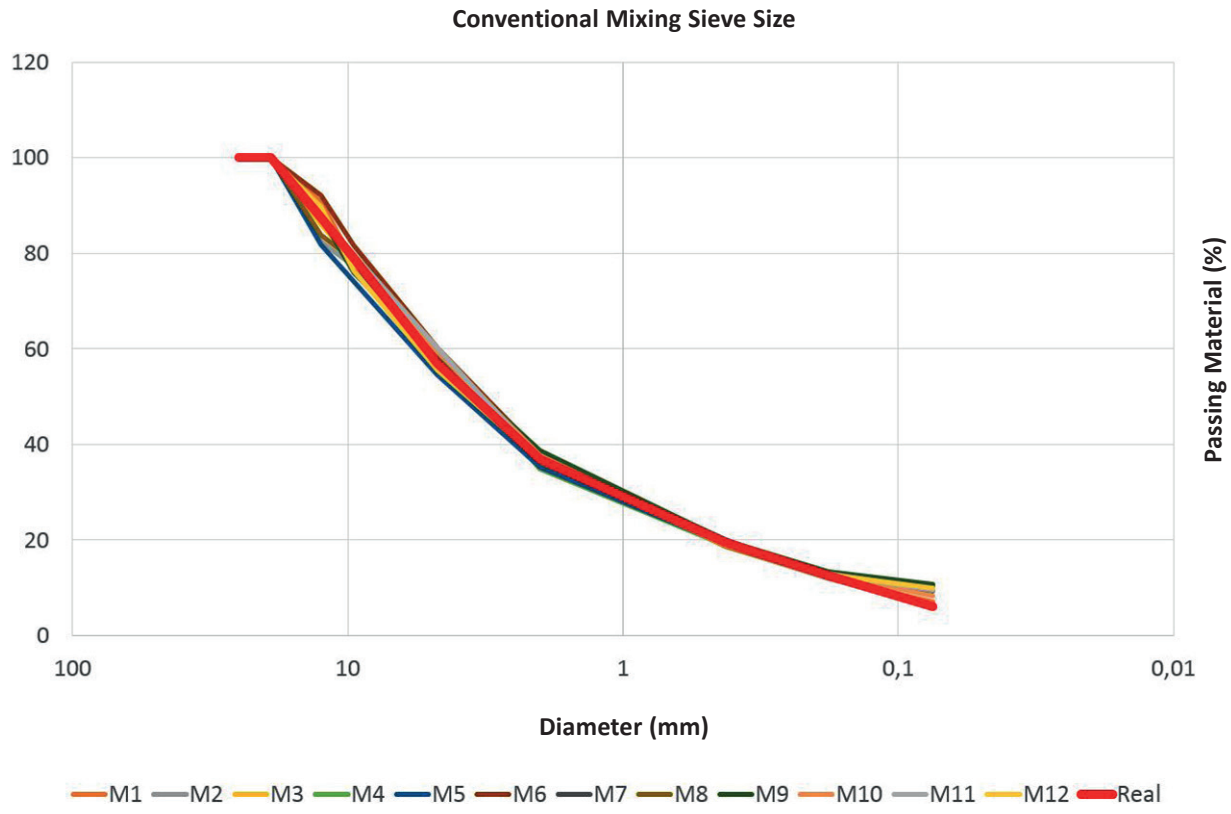

Fig. 10. Sieve size reconstruction for conventional samples

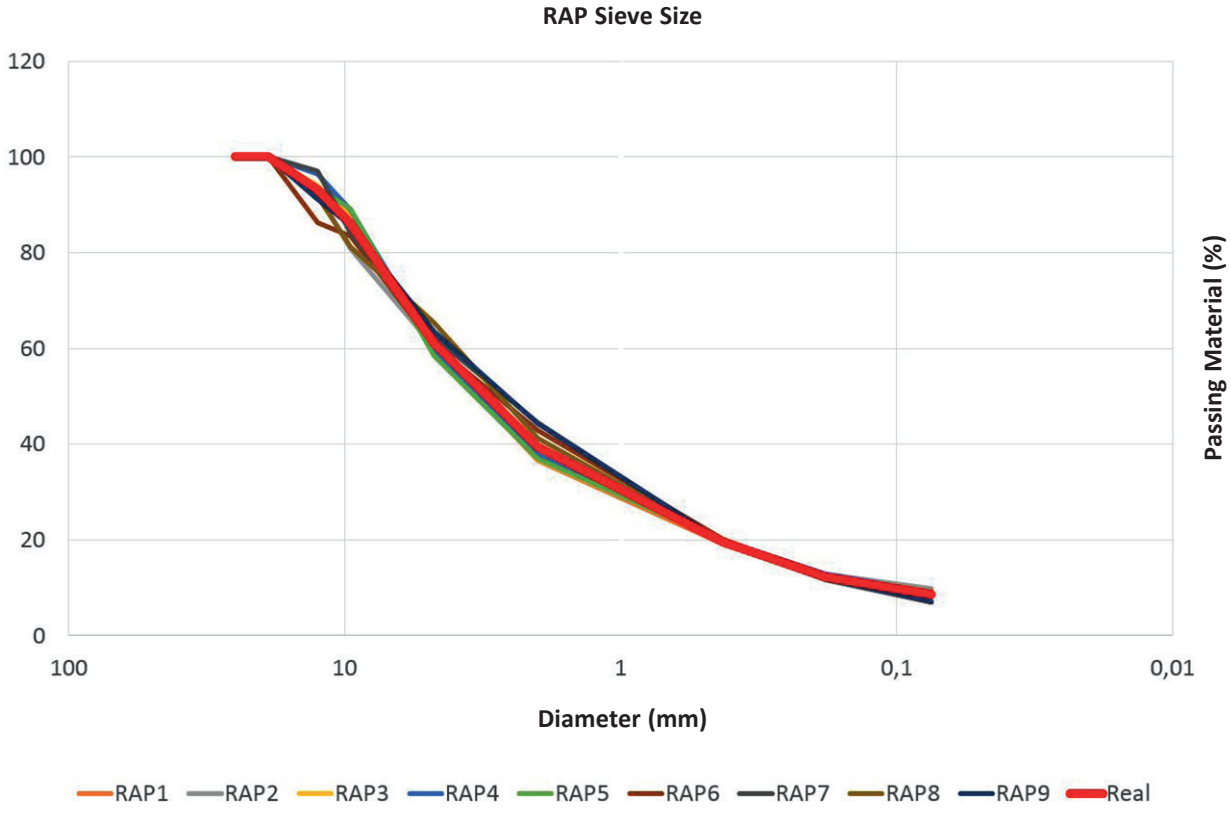

Fig. 11. Sieve size reconstruction for RAP samples

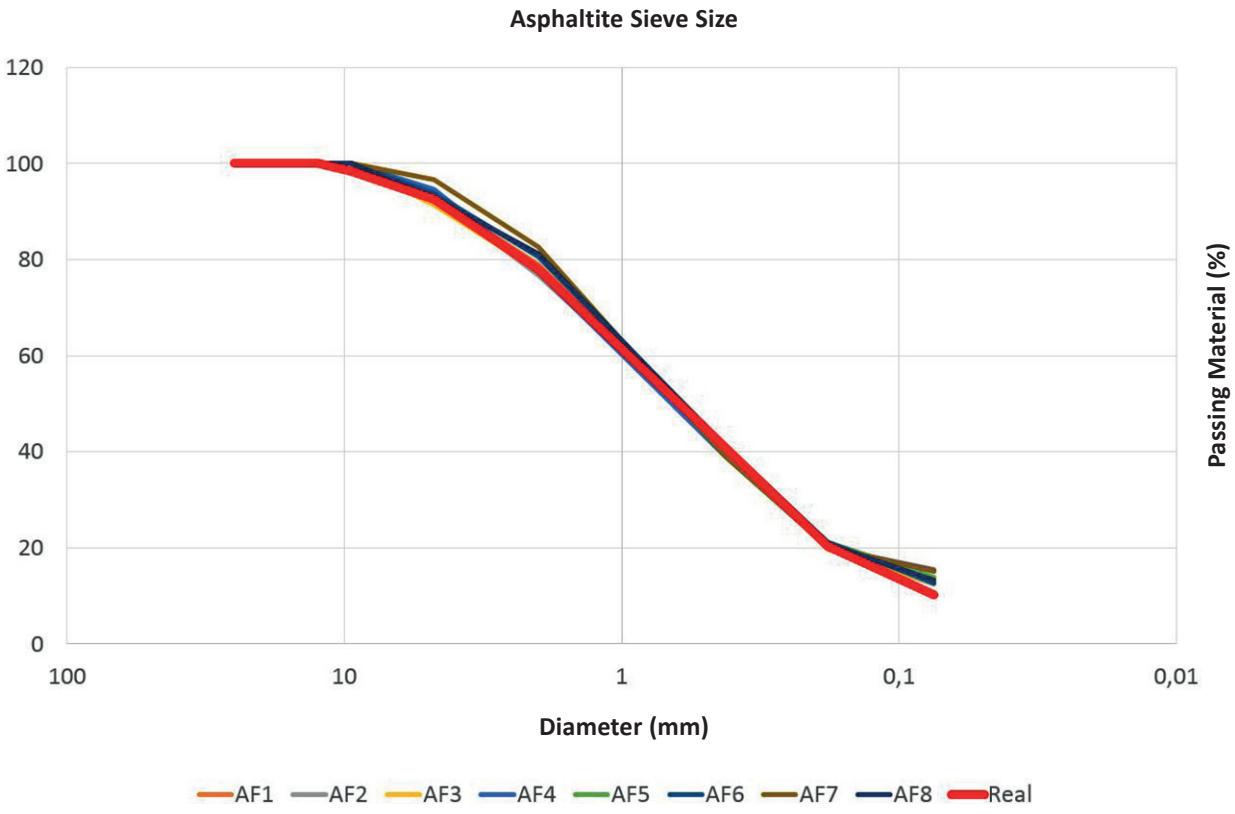

Fig. 12. Sieve size reconstruction for asphaltite samples

average in sieve No. 200. The particles of 0.075 mm in size cannot be detected so easily. This is seen in graphs 8, 9 and 10, where the curves diverge in the last sieve.

4. Conclusions

The segmentation model for dense-graded asphalt mixtures presented in this paper demonstrates the use and versatility of digital image processing for particle discrimination within a material. The algorithm segments particles larger than 0.0324 mm^2 of area with a lower average error of up to 3%. In future works, the image acquisition can be improved to obtain a better definition of the elements and thus to segment inferior areas. To optimize the method, it is necessary to include a larger number of samples to analyze and apply artificial intelligence techniques within the algorithm to make it more efficient for the discrimination of particles.

The sieve size reconstruction performed in this work not only presents a functional model for segmentation of the aggregate but also presents a digital tool with a wide field of application for civil engineering in pavements. One field of use in the area of geotechnics can be, for instance, as a quality control system for road construction or as a support tool in road design.

Implementation of the watercolor filter eliminates two critical points in aggregate segmentation, i.e. color discrimination and contact points. This is because it is a specialized contours detection filter. The method developed in this work is thus not affected by dark or multicolored aggregate. Even when two particles share the same border.

Meanwhile, morphological operations help separate elements joined together by the noise generated during acquisition of the image or the lack of resolution in the camera. In the development of this work, the opening operation was used to separate the aggregate and showed promising results for the segmentation. This operation presents a problem in the definition of the dimension of the structural element size, since oversizing causes the elimination of work material. For this reason, the integration of this type of operations with modern techniques of artificial intelligence is proposed to improve the selection of structural elements in a flexible manner and at low computational cost.

Acknowledgments. The authors wish to thank the Vice-Rector for research at the Nueva Granada Military University, in particular for the financing of the high impact research project IMP-ING-2132.

References

[1] F. Bianconi, F. Di Maria, C. Micale, A. Fernández, and R.W. Harvey, "Grain-size assessment of fine and coarse aggregates through bipolar area morphology," *Mach. Vis. Appl.*, vol. 26, no. 6, pp. 775–789, 2015.

[2] F. Di Maria, F. Bianconi, C. Micale, S. Baglioni, and M. Marionni, "Quality assessment for recycling aggregates from construction and demolition waste: An image-based approach for particle size estimation," *Waste Manag.*, vol. 48, pp. 344–352, 2016.
[3] J. Han, K. Wang, X. Wang, and P.J.M. Monteiro, "2D image analysis method for evaluating coarse aggregate characteristic and distribution in concrete," *Constr. Build. Mater.*, vol. 127, pp. 30–42, 2016.
[4] A.J. Ramme, K. Voss , J. Lesporis, M.S. Lendhey, T.R. Coughlin, E.J. Strauss, and O.D. Kennedy, "Automated Bone Segmentation and Surface Evaluation of a Small Animal Model of Post-Traumatic Osteoarthritis," *Ann. Biomed. Eng.*, vol. 45, no. 5, pp. 1227–1235, 2017.
[5] M. Abhik, C. Debashish, B. Kousik, and H. Arpan, "Development of a mass model in estimating weight-wise particle size distribution using digital image processing," *Int. J. Min. Sci. Technol.*, vol. 27, pp. 435–443, 2017.
[6] J.S. Athertya and G. Saravana Kumar, "Automatic segmentation of vertebral contours from CT images using fuzzy corners," *Comput. Biol. Med.*, vol. 72, pp. 75–89, 2016.
[7] S. Yin, Y. Qian, and M. Gong, "Unsupervised hierarchical image segmentation through fuzzy entropy maximization," *Pattern Recognit. J.*, vol. 68, pp. 245–259, 2017.
[8] W. Wang, C. Wu, C. Wu, and W. Regression, "Image Segmentation by Correlation Adaptive Weighted Regression," *Neurocomputing*, vol. 17, 2017.
[9] P. Zarychta, P. Badura, and E. Pietka, "Comparative analysis of selected classifiers in posterior cruciate ligaments computer aided diagnosis," *Bull. Pol. Ac.: Tech.*, vol. 65, no. 1, 2017.
[10] C.G. Berrocal, I. Löfgren, K. Lundgren, N. Görander, and C. Halldén, "Characterisation of bending cracks in R/FRC using image analysis," *Submitt. to Mater. Struct.*, vol. 90, pp. 104–116, 2016.
[11] I. Michalska-Pożoga, R. Tomkowski, T. Rydzkowski, and V.K. Thakur, "Towards the usage of image analysis technique to measure particles size and composition in wood-polymer composites," *Ind. Crops Prod.*, vol. 92, pp. 149–156, 2016.
[12] A. Stankiewicz, T. Marciniak, A. Dąbrowski, M. Stopa, P. Rakowicz, and E. Marciniak, "Denoising methods for improving automatic segmentation in OCT images of human eye," *Bull. Pol. Ac.: Tech.*, vol. 65, no. 1, 2017.
[13] G. Vladic, S. Dedijer, L. Koltai, I. Juric, and N. Kašikovic, "Image processing based quality control of coated paper folding," *Measurement*, vol. 100, pp. 99–109, 2017.
[14] M. Mejía and M. Alzate, "Clasificación automática de formas patológicas de eritrocitos humanos Automatic classification of pathological shapes in human erythrocytes," *Rev. Ing.*, vol. 21, no. 1, pp. 31–48, 2015.
[15] K. Espinoza, D.L. Valera, J.A. Torres, A. López, and F.D. Molina-aiz, "Combination of image processing and artificial neural networks as a novel approach for the identification of Bemisia tabaci and Frankliniella occidentalis on sticky traps in greenhouse agriculture," *Comput. Electron. Agric.*, vol. 127, pp. 495–505, 2016.
[16] A. Tedeschi and F. Benedetto, "A real-time automatic pavement crack and pothole recognition system for mobile Android-based devices," *Adv. Eng. Informatics*, vol. 32, pp. 11–25, 2017.
[17] H. Yoo and Y. Kim, "Development of a Crack Recognition Algorithm from Non-routed Pavement Images using Artificial Neural Network and Binary Logistic Regression," *KSCE J. Civ. Eng.*, vol. 20, pp. 1151–1162, 2016.
[18] C. Sha, J. Hou, and H. Cui, "A robust 2D Otsu's thresholding method in image segmentation q," *J. Vis. Commun. Image R. J.*, vol. 41, pp. 339–351, 2016.
[19] S.M.E. Harb, N. Ashidi, M. Isa, and S.A. Salamah, "Improved image magnification algorithm based on Otsu," *Comput. Electr. Eng. J.*, vol. 46, pp. 338–355, 2015.
[20] S. Mohammad, A. Hasan, and K. Ko, "Depth edge detection by image-based smoothing and morphological operations," *J. Comput. Des. Eng.*, vol. 3, pp. 191–197, 2016.
[21] S.R. Borra, G.J. Reddy, E.S. Reddy, J. Reddy, and S. Reddy, "Classification of Fingerprint Images with the aid of Morphological Operation and AGNN Classifier," *Appl. Comput. Informatics*, 2017.
[22] J.E. Arco, J.M. Górriz, J. Ramírez, I. Álvarez, and C.G. Puntonet, "Digital image analysis for automatic enumeration of malaria parasites using morphological operations," *Expert Syst. Appl.*, vol. 42, pp. 3041–3047, 2015.
[23] R.C. Gonzalez and R.E. Woods, *Digital Image Processing*, vol. 21. Pearson Education, 2011.
[24] X. Bai, "Morphological center operator based infrared and visible image fusion through correlation coefficient," *Infrared Phys. Technol.*, vol. 76, pp. 546–554, 2016.